

The Active Optics System for the Discovery Channel Telescope

Byron Smith^{*a}, Tomas Chylek^a, Brian Cuerden^b, Bill DeGross^a,
Paul J. Lotz^a, Alexander Venetiou^a

^aLowell Observatory, 1400 W. Mars Hill Road, Flagstaff, AZ 86001;

^bUniversity of Arizona College of Optical Sciences, 1630 E. University Blvd., Tucson, AZ 85721

ABSTRACT

The Discovery Channel Telescope (DCT) is a 4.3-meter telescope designed for dual optical configurations, featuring an f/6.1 Ritchey-Chretien prescription with a 0.5° field-of-view, and a corrected f/2.3 prime focus with a 2° field-of-view. The DCT Active Optics System (AOS) maintains collimation and mirror figure to provide seeing limited images across the focal planes and rapid settling times to minimize observing overhead, using a combination of feed-forward and low-bandwidth feedback control via wavefront sensing. Collimation is maintained by tip-tilt-piston control of the M2 assembly and articulating M1 within its cell, taking advantage of the 120 degree-of-freedom support used for figure control. We present an overview of the AOS design and principles of operation, and a summary of progress and results to date.

Keywords: DCT, Lowell Observatory, Active Optics, opto-mechanics, wavefront control

1. INTRODUCTION

The Active Optics System (AOS) for the Discovery Channel Telescope (DCT) is responsible for maintaining the figure and collimation of the telescope optics and consequently plays a major role in the quality of the images delivered for science. The AOS consists of active supports for the primary and secondary mirrors, the controls for those supports, and an overarching control system which commands the individual mirror supports to maintain the wavefront quality based on calibration data and feedback from a wavefront sensor. This paper describes these components, and their development as part of the DCT project, including the performance and figure control analysis for the primary mirror.

DCT requirements to support large instrument payloads at both prime and Ritchey-Chretien foci, and high-cadence observations for survey work, drive some notable features of the AOS. In the prime focus configuration, collimation is achieved by articulating the primary mirror on its support. This created a challenge to extend the performance of the support from a single nominal operating position to a significant range of travel, but also takes advantage of otherwise required hardware and eliminates the need for an active positioner for the prime focus instrument. To support high-cadence observations, short settling times (<8 seconds) after a telescope move are required. This is accomplished by utilizing mirror support bandwidths comparable to the mount control bandwidth, driven by a combination of feed-forward control based on calibration data and low-bandwidth wavefront feedback. When not driven by requirements, novel approaches were generally avoided, relying instead on proven strategies for accomplishing goals.

2. AOS OVERVIEW

The DCT Active Optics System (AOS) maintains collimation and mirror figure to provide seeing limited images. The AOS can operate open loop and closed loop. Open loop AOS operation maintains collimation and M1 mirror figure with operational parameters and calibration data. Closed loop AOS operation maintains collimation and M1 mirror figure with operational parameters, calibration data, and wavefront data. See Figure 1 for the M1 portion of the AOS.

* bsmith@lowell.edu; phone: 928-233-3258; fax: 928-233-3268; lowell.edu



Figure 1. AOS M1 assembly and testing with mirror simulator

In open loop operation, the AOS uses operational parameters: ambient temperature, M1 temperature, mount temperature, and zenith angle as inputs to the look up tables (LUTs).

The AOS will process mount zenith angle and temperature changes every 50 ms. This is the same rate as the mount demanded positions are updated. The open and closed loop performances vary due to gravity induced deformations that are uncorrelated but repeatable. See Figure 2 for open loop M1 figure control performance requirement. Section 8.6 shows open loop analysis results.

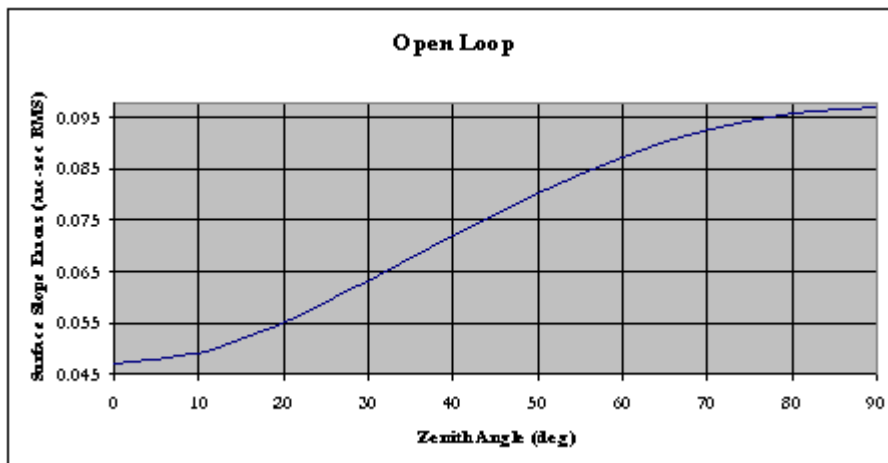


Figure 2. AOS M1 Figure Control Performance Requirement

In closed loop operation, the AOS uses the open loop LUTs as well as wavefront sensor feedback. The LUTs are used for the majority of the correction with the wavefront sensor providing fine adjustments. The AOS receives both Zernikes and bending mode correction coefficients from the wavefront sensor. The AOS uses Zernike 4 (focus), 7, and 8 (coma) for collimation corrections. The AOS uses 26 bending modes for M1 figure correction. The AOS will receive a decomposed wavefront every 30 seconds. The closed loop bandwidth is approximately 0.01 Hz. See Figure 3 for closed loop M1 figure control performance requirement. Section 8.6 shows the closed loop analysis results.

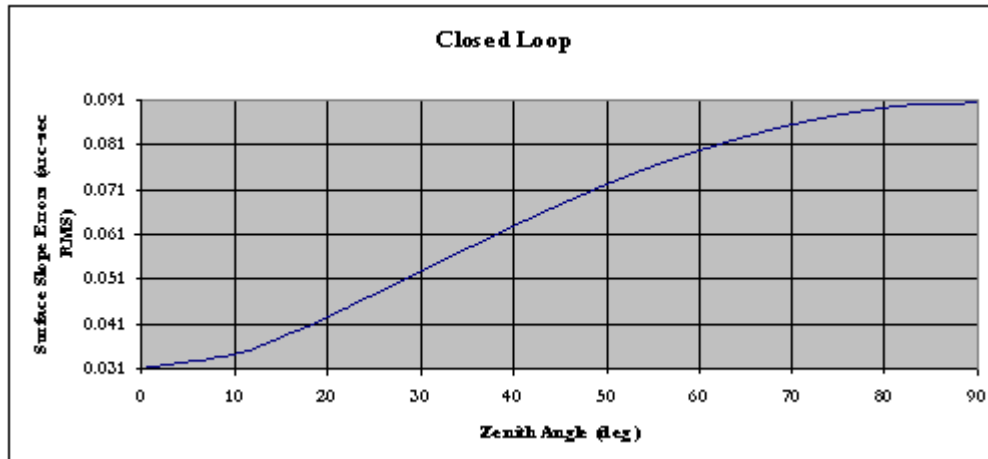


Figure 3. AOS M1 Figure Control Performance Requirement

The M2 surface slope errors due to support force errors are required to be less than 0.021 arc-sec RMS.

DCT has two optical configurations: Richey-Chretien (RC) and Prime Focus Assembly (PFA). In the RC configuration, the M2 axial supports correct for collimation errors. In the PFA configuration, the PFA does not have active supports so the M1 axial supports correct for collimation errors. In both configurations, the M1 corrects for the M1 figure error.

For controls and software, there are three main components: Active Optics Control System (AOS), M1 Control System (M1S), and M2 Control System (M2S). The AOS accepts the wavefront sensor feedback and combines it with the LUT feed-forward demands. The demands are sent to the M1S and M2S as bending modes and x-tilt/y-tilt/piston positions. The AOS also sends a pointing offset to the TCS based on the coma correction.

The M1S accepts demands from the AOS. The M1S sends position demands to the M1 axial support position loop (M1P). The M1S converts the 26 bending modes to a 120 axial support force suite. It also combines the force demands from the M1P with the bending mode force demand suite. The combined force demand suite is sent to the M1 axial support force loop (M1F). The M1F includes all the hardware to move the axial supports. The M1S also includes the M1 Lateral Support Control System (M1L). The M1L accepts force demands from the M1S. Nominally, the M1S force demand to the M1L is zero. The M1L maintains the M1 mirror centration at all zenith angles with 36 active pneumatic actuators and feedback from three passive tangent definers and their force transducers.

The M2S accepts x-tilt/y-tilt/piston demands from the AOS. The M2S converts the demands into actuator position demands. The actuator position demands are sent to the M2 axial support position loop (M2P). The M2P includes all the hardware to move the axial supports. The M2S also includes the M2 Vacuum Control System (M2V). The M2V accepts force demands from the M2S. Nominally, the M2S force demand to the M2V is zero. The M2V maintains zero force on the M2 mirror at all zenith angles with feedback from three force transducers on the M2 cell structure.

3. OPTO-MECHANICS

3.1 Primary mirror supports and auxiliary systems

The primary mirror (M1) made out of Ultra Low Expansion (ULE) glass, is supported in the telescope by 120 axial electro-mechanical and by 36 lateral pneumatic actuators at the outer diameter of the mirror arranged into a Schwesinger type support.¹ The geometry pattern is shown in Figure 4 (lateral supports) and Figure 5 (axial supports) and has been optimized by College of Optical Sciences at University of Arizona. The telescope optical performance is enhanced by polishing the mirror on identical support system to remove the zenith pointing gravity effects. The final optimized axial support pattern arranged in five concentric circles is shown in Figure 5. The lateral position of the mirror is defined by three tangential definers equally spaced on the outer diameter of the mirror. The opto-mechanical design also includes active thermal management of the mirror in order to satisfy the local mirror seeing requirements.

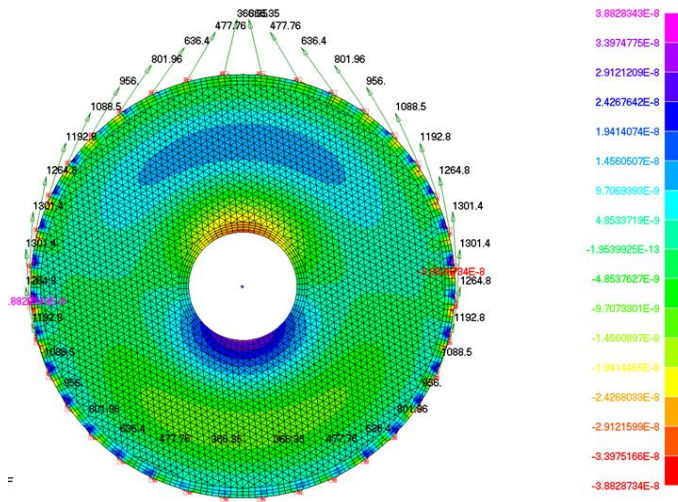


Figure 4. FEA Analysis of the Schwesinger Supports (Courtesy of College of Optical Sciences, UofA)

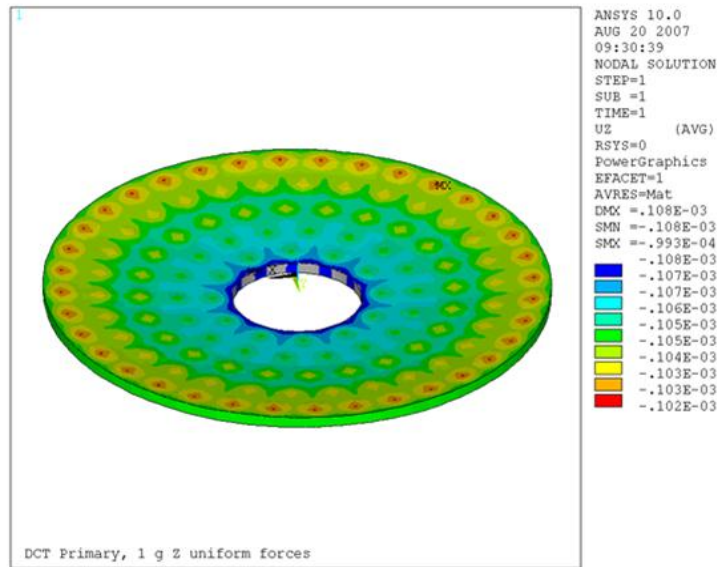


Figure 5. Axial Supports Glass Stress Prediction (Courtesy of College of Optical Sciences, UofA)

Figure 6 shows the detail of arrangement of the axial and lateral supports on the mirror cell with the mirror simulator. The axial supports incorporate electro-mechanical stepper motors with harmonic drive and a ball screw. The assembled axial support is shown in Figure 7 and includes an S-shaped load cell for local force control loop. The axial support allows total 7mm linear travel with 0.1um resolution. The connection to the mirror features a spring loaded detent attached to the back side of the mirror which provides tool-free assembly and disassembly. Titanium alloy flexures allow up to 9.5mm lateral motion each way. The design also includes bi-directional force limiting mechanism. In tension, the glass is protected by the spring loaded detents limiting maximum pull force to less than 60lbs. In compression, the design includes a spring loaded mechanism limiting maximum force to 150lbs at the maximum travel.

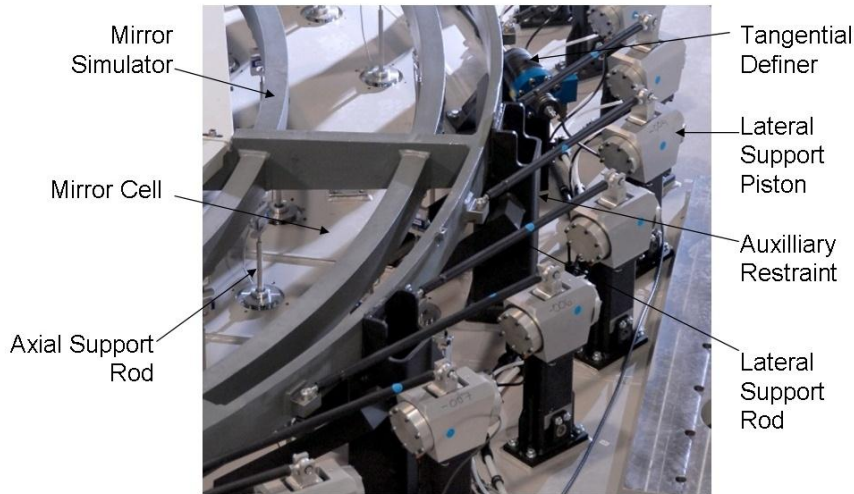


Figure 6. Arrangement of the lateral and axial supports.

Thirty-six lateral supports are arranged in a configuration based on Schwesinger design with $\beta=0.76$. The supports are using double-acting pneumatic cylinders with rolling Bellofram diaphragms providing $\pm 0.25''$ travel at the end of the lever which is pivoted in Riverhawk single ended flexures. Connecting rods of varying lengths fitted with Titanium flexures and ball joints are used to transfer the forces from the air pistons to the mirror. Figure 8 shows the lateral support mounted on the mirror cell (left) with its connecting rod spanning over the tangential definer with a blue load cell (right). The lateral supports are using preload pressure of 15 psi and are actively regulated to 15-72psi on high pressure side depending on the telescope Zenith distance and the tangential definers load cell feedback.



Figure 7. Axial Support Assembly

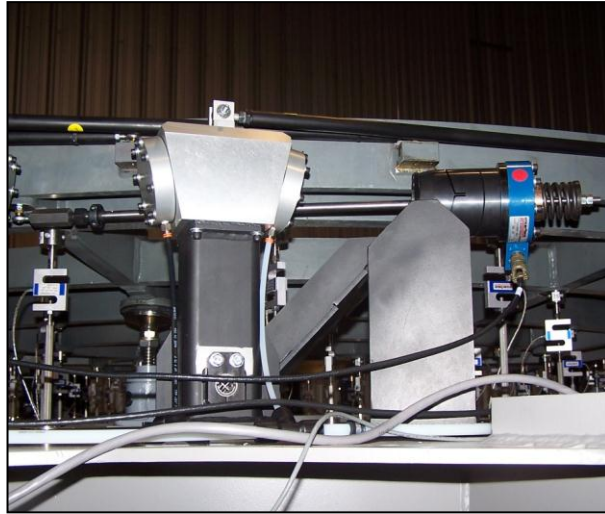


Figure 8. Lateral Support and Tangential Definer Assembly

Three tangent definers passively constrain X and Y (decenter) position of the mirror and its rotation about optical axis. These are high stiffness components, equally spaced near the outer diameter of the mirror and allow precise manual adjustment for alignment. Each one is fitted with a load cell, tension/compression force limiting mechanism and two sets of flexures.

Four incremental length gages Heidenhain MT1271 along with four GHSIR 750 LVDT spring loaded position sensors (repeatability error $<2.5\mu\text{m}$) as shown in Figure 9 are placed at the mirror OD and are used to determine M1 tip/tilt and piston positions. Four Invar pucks which are attached to the mirror OD provide attachment point for the measuring contact of the Heidenhain gages and are also used to support sphere mounted retro-reflectors (SMR) for laser tracker aided alignment.



Figure 9. Position Sensor Assembly

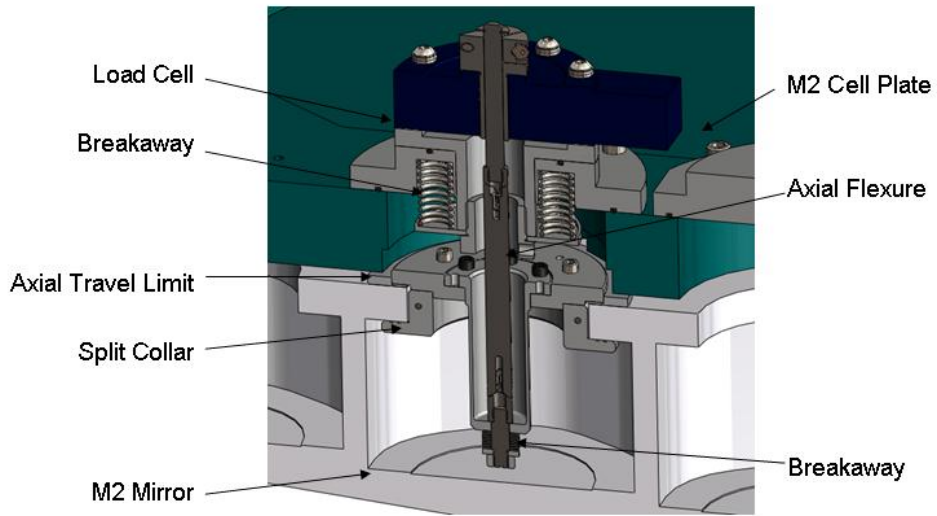


Figure 11. Secondary Mirror Axial Post

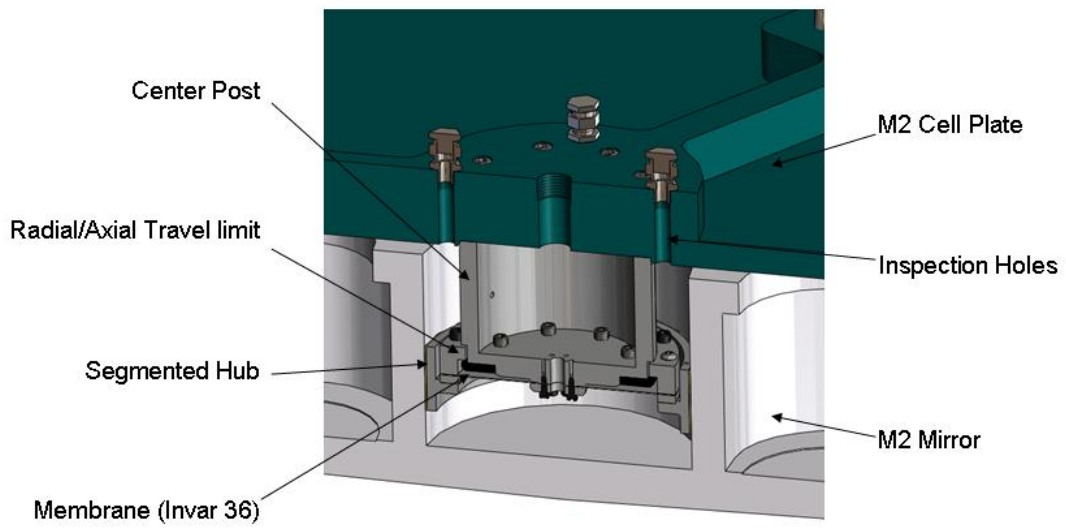


Figure 12. Secondary Mirror Center Post

Rotational position of the mirror is defined by a metal tangential strap incorporated in one of the axial posts. To maintain vacuum, the mirror is sealed on its outer edge with silicone rubber seal ring. The vacuum system is controlled to keep the post reactions down below 1lb in order to satisfy the surface distortion requirements. When the vacuum system is not operating the full weight of the mirror is supported by the axial posts. Two independent pressure relief valves provide safety of the mirror in case of the pressure/vacuum failure. There are also three external travel limits which limit M2 movement in the cell in axial and lateral directions to prevent damage of the flexures and the glass.

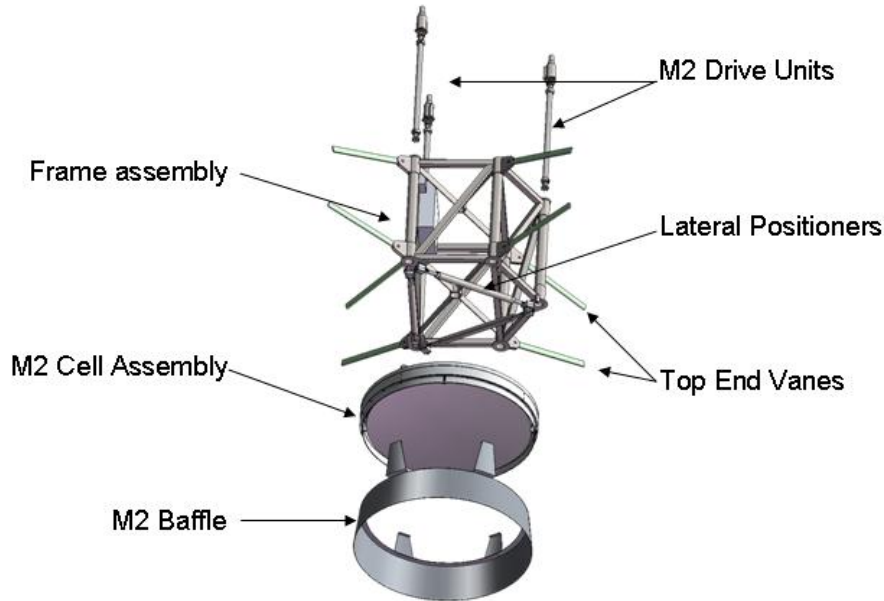


Figure 13. Secondary Mirror Top End Assembly

As shown in Figure 13 the mirror cell assembly is suspended on three lateral positioners and precisely actuated in piston and tilt using three electromechanical (harmonic gear) actuators. Three incremental length gages Heidenhain MT1271 along with three GHSIR 750 LVDT spring loaded position sensors monitor position of the cell assembly in axial direction.

4. ELECTRONICS

The DCT AOS electronics uses National Instruments (NI) compact Reconfigurable Input/Output (cRIO) hardware for most of the I/O and control. The hardware subsystems are the M1F, M1L, M1P, M2V, and M2P. After the I/O has been acquired by the cRIO, all communications to other subsystems is with TCP/IP. The subsystems that do not have hardware I/O use industrial rack-mounted PCs. These subsystems are the AOS, M1S, and M2S. Figure 14 shows the AOS network topology.

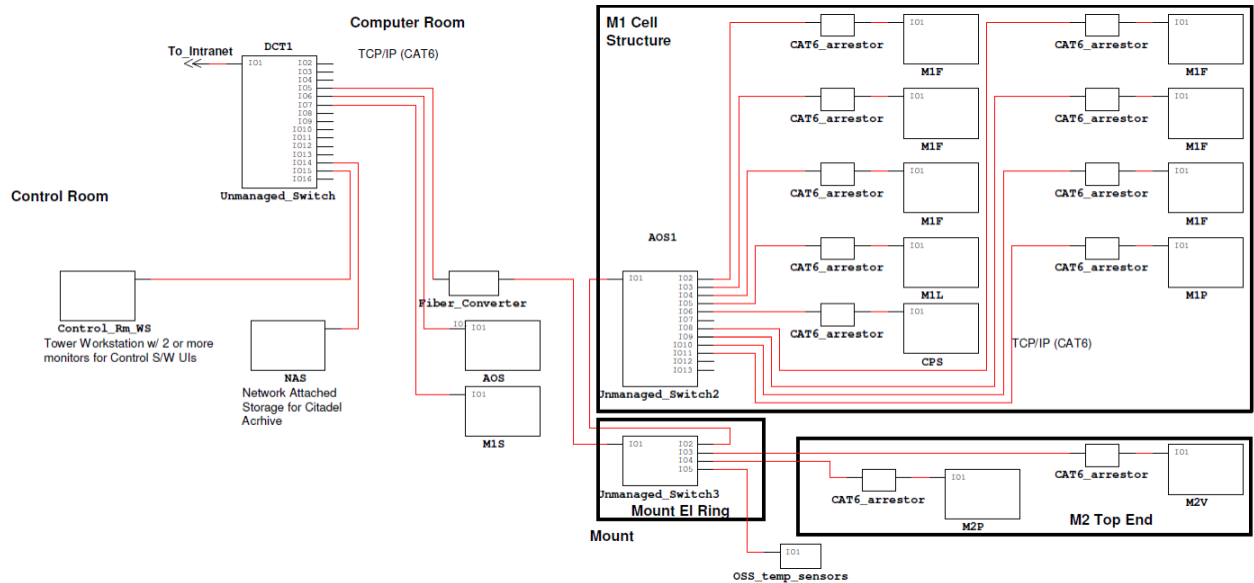


Figure 14. AOS Network Topology

4.1 Primary Mirror Axial Support Force Loop Control (M1F)

There are six M1Fs in the AOS. Each M1F controls 20 axial support actuators. M1F maintains the demanded force on each axial support by stepping the axial support stepper motor. The M1F receives a force measurement from its respective axial support force transducer. M1F uses the force measurement to determine the number of steps required to maintain the demanded force. There are a total of 20 axial supports per cRIO. There are a total of six cRIOs to control 120 actuators.

4.2 Primary Mirror Lateral Support Control (M1L)

The lateral supports are controlled independently of the axial supports. The lateral supports consist of 36 pneumatic actuators. The pneumatic actuators share one pneumatic control circuit with one pressure regulator. The lateral supports use three passive tangent definers with force transducers as feedback. For safety, the M1L monitors delta pressure to determine if the system should be shut down.

4.3 Primary Mirror Axial Support Position Loop Control (M1P)

The M1P reads the four position sensors and calculates the x-tilt, y-tilt, and piston components. X-tilt, y-tilt, and piston are converted to M1F force demands. M1P generates a force demand for each axial support M1F. For homing, M1P uses 4 absolute position sensors to determine which way to move to reach the relative position sensors reference marks .

4.4 Secondary Mirror Vacuum Control (M2V)

The M2V controls two vacuum (fine and coarse) and two pressure (fine and coarse) solenoid valves. The M2V reads measurements from three force transducer and one delta pressure transducer. M2V receives force measurements from three force transducers. M2V uses the force measurements to determine if the solenoid valves should be open or closed. A delta pressure transducer is provided for safety.

4.5 Secondary Mirror Axial Position Control (M2P)

The M2P reads the six position sensors (3 - absolute and 3 - relative) and calculates the x-tilt, y-tilt, and piston components. X-tilt, y-tilt, and piston are converted to position demands. M2P generates a position command for each axial support. The 3 absolute position sensors are used to determine the relative position sensor reference marks for the homing routine. Figure 15 shows the AOS control block diagram.

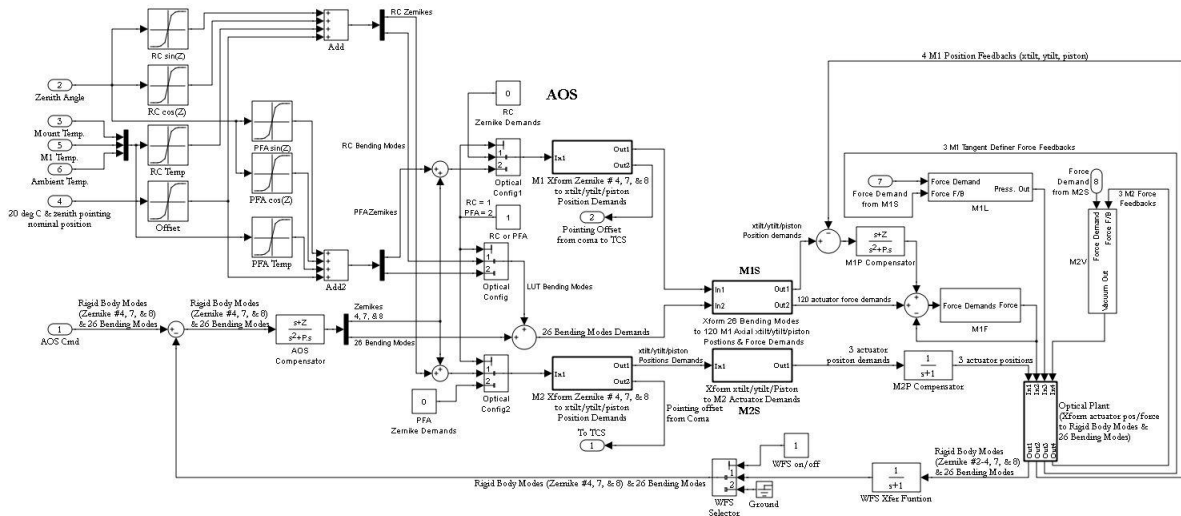


Figure 15. AOS Control Block Diagram

5. SOFTWARE

The DCT software design allocates particular functionalities to each of a number of stand-alone data-driven components. For a further discussion of the component concept, the software technologies we mention in this paper, and the DCT software development process (see Lotz paper).²

In particular, the AOS software components are as follows (see Figure 16).

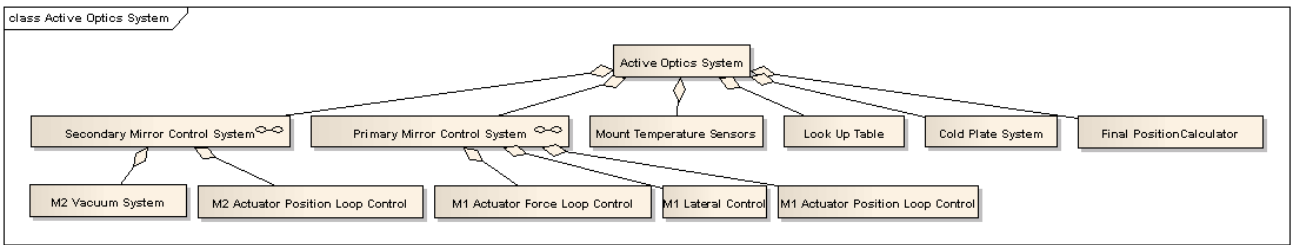


Figure 16. AOS Components

Each component has a summary state and a detailed state. The allowed summary states and their relationships appear in Figure 17.

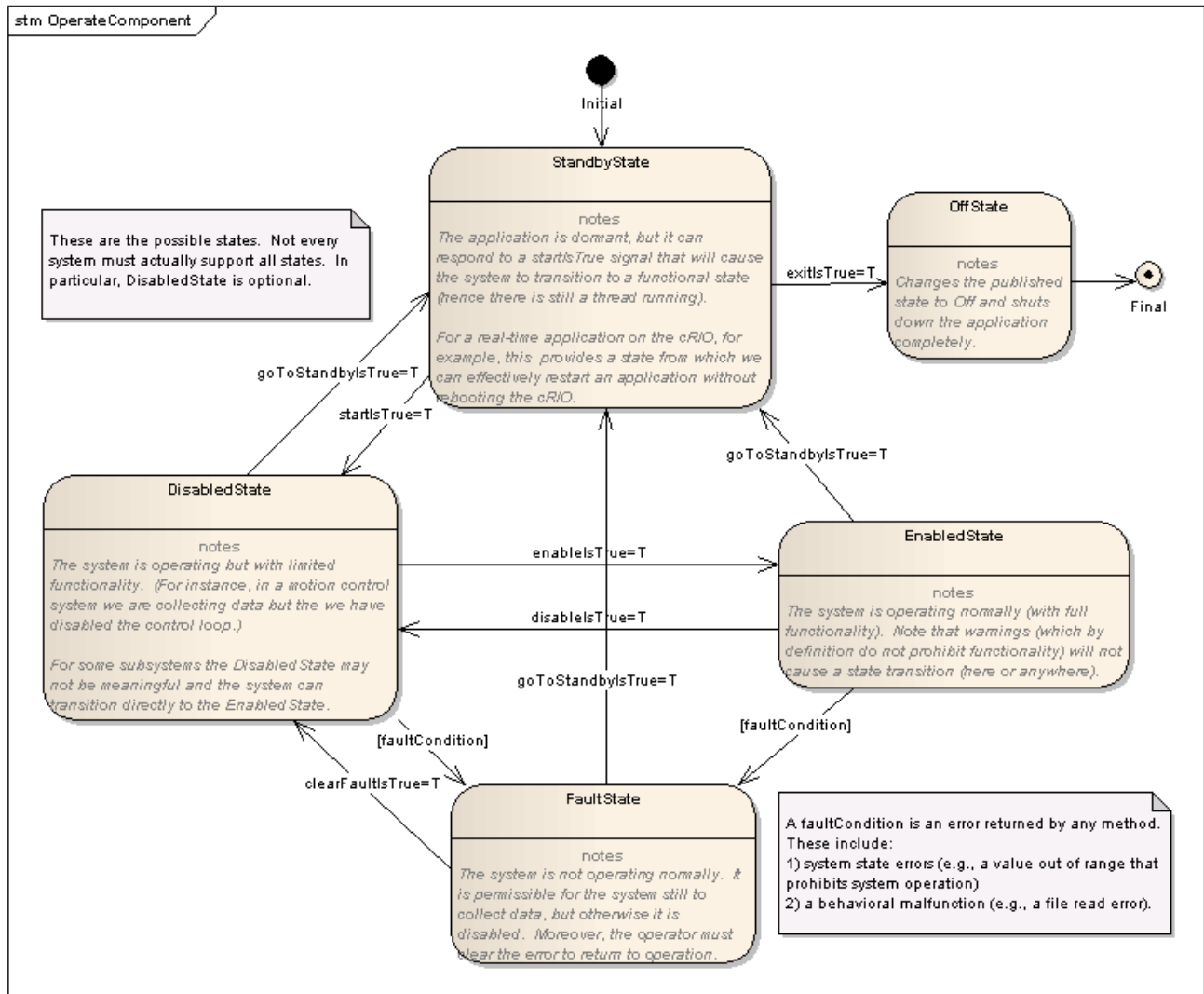


Figure 17. Summary States.

Summary states apply hierarchically—that is, if a component has subcomponents it takes into account the summary state of its subcomponents when determining its own summary state.

The list of available detailed states, on the other hand, is generally particular to a component, and captures the state design for the successful operation of the component. For instance, Figure 18 shows the possible states for the M1 Actuator Position Loop Control. Further, each of a component’s detailed states maps to exactly one summary state.

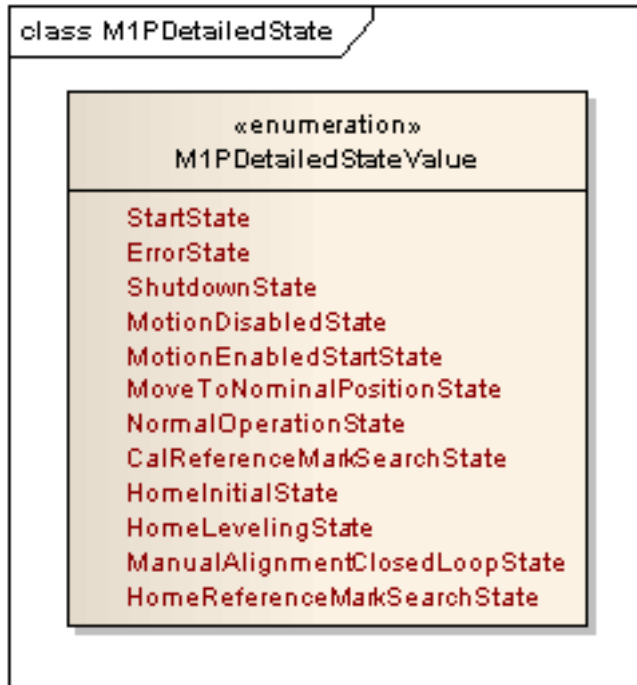


Figure 18. Primary Mirror Axial Support Position Loop (MIP) detailed states.

Communication between components—as well as within a component between its Views and Controller—is via the National Instruments Publish-Subscribe Protocol using networked shared variables. Networked communication permits communication between widely spaced applications with minimal hardware requirements. Moreover, an application may deploy on any networked target that has the hardware that application requires. The publish-subscribe paradigm allows for multiple subscribers to a message. Subscribers include one or more Views or Controllers. For instance, the Controller for a particular component may publish status information that is of interest to the View for that component as well as to the Controller and View of the next higher-level component in the software hierarchy. We configure the communication application to log messages to a Citadel historical database.

The controllers for each of the Primary Mirror Control System and Secondary Mirror Control System subcomponents run on the real-time processor of a National Instruments compactRIO device. The real-time controllers interface to a Field Programmable Gate Array configured to perform input/output and other hardware processing operations. The software team writes desktop, real-time, and FPGA applications using the National Instruments LabVIEW graphical programming environment.

6. INTEGRATION AND TESTING

As of May 2010, significant progress in mechanical integration and subsystem testing has been made. As a risk mitigation measure, the M1 axial support, lateral support, and M2 vacuum support pneumatic system were tested in 2008 and 2009 using prototype hardware. These tests validated the basic design approach, confirmed basic functionality, measured critical performance parameters, and tested the low temperature and life capabilities of the hardware.

Production of the M1 supports began in October, 2009 with assembly of the 120 M1 axial supports. Unit acceptance testing was completed in mid-December 2009. Assembly and test of the 36 lateral supports followed. The M1 Cell was received from GDST in late December and installation of the supports hardware began immediately (see Figure 19).



Figure 19. Mirror Supports Installation on M1 Cell

Considerable effort was also spent in the layout and installation of the electronics harnesses and controls enclosures (see Figure 20).

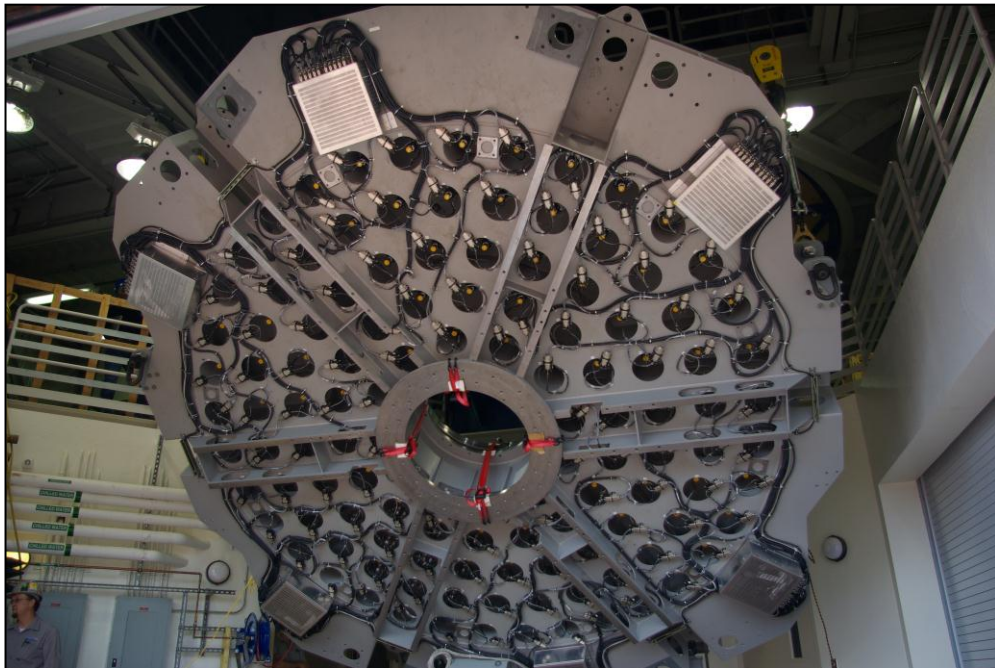


Figure 20. M1 Cell cable harnesses and controls

By February, 2010, we reached the stage of applying power and initial checkout of the supports and controls. In April we had demonstrated closed-loop force control of 120 axial supports simultaneously, and have closed the axial support position loop and lateral support force loop. Remaining tests include demonstration of the homing routine for the axial supports, functional tests of the M1 Supports supervisory software, referred to as “M1S,” and performance tests and tuning of the controls parameters in the M1 subsystem configuration. Due to the schedule for the mount installation, this testing will not be completed until after the mount is accepted from GDST and the mount installer.

Upon completion of the aforementioned tests and tuning at the subsystem (cell) level, we will prepare for and conduct testing at the system level – without glass. The AOS system will be exercised using a mass simulator for M1, visible in Figure 19, and a simulator for the M2/Cell combined mass, Figure 21. In this configuration, we can test the motion control capabilities needed for collimation, but not figure control. Both mirror simulators are rigid steel fixtures which are not designed to simulate the stiffness of the real mirrors. In addition, the configuration of the M2 simulator does not allow the vacuum figure control system to be tested.



Figure 21. M2 Top End showing M2 frame and simulator

After the first AOS system test, we will remove the mirror simulator from the M1 cell and remove the M2 simulator from the top end. The coated M1 will be installed in the cell. The M1 Cell assembly will then be installed in the mount. The M2 top end will be installed in the mount without the mirror or simulator, since the real M2 will not be available until early 2011. In this configuration, we intend to perform tests of the AOS in a “prime focus” configuration. Using one of the guider probes developed for the DCT Guider and Wavefront Sensing System (GWAVES) located near the prime focus, we will perform engineering tests intended to evaluate the primary mirror optical performance and test the capabilities of the AOS to control the mirror figure. At the same time, we will gain valuable experience operating the GWAVES system including the interface of GWAVES with the AOS.

We expect the process of figuring the secondary mirror to be complete in early 2011. Upon receiving the M2, we will assemble it into the M2 Cell and install the assembly in the top end. With both mirrors now installed in the mount, we will conduct a second system test of the AOS. This will be the first opportunity to evaluate the system’s performance in collimation and figure control. A period of system testing, debugging, and optimization is expected before the telescope system is ready for an acceptance test, which is currently planned for August, 2011.

7. ANALYSIS: MINIMIZATION OF SURFACE RMS DISTORTION

In this section we describe the method used to determine the coefficients, Φ , of a set of surface shapes that minimize the RMS surface slopes when added to a distorted surface shape, U_g .

Equation 1 is the expression for the sum square surface distortion after subtracting m shapes that may not be orthogonal to each other. The minimization operation, setting the partial derivative of Equation 1 with respect to each of the shape coefficients, results in Equation 2 which is readily solved for the shape coefficients, Equation 3.

Equation 1

$$U_{ss} = (\vec{U}_g - \vec{\Phi}[L])^T (\vec{U}_g - \vec{\Phi}[L]) = \vec{U}_g^T \vec{U}_g - 2\vec{\Phi}[L]\vec{U}_g^T + \vec{\Phi}[L][L]^T \vec{\Phi}^T$$

Where:

- U_{ss} is the square of the net surface distortion
- U_g is a $1 \times m$ vector of surface displacements (the load case to be minimized).
- Φ is a $1 \times n$ vector of shape function coefficients.
- L is an $n \times m$ matrix of n shape functions.

Minimizing U_{ss} wrt Φ ;

Equation 2

$$\frac{\partial U_{ss}}{\partial \Phi} = 0 = -2[L][L]^T \vec{\Phi} + 2[L]\vec{U}_g$$

Solving equation 2 for Φ gives;

Equation 3

$$\vec{\Phi} = [[L][L]^T]^{-1}[L]\vec{U}_g$$

This method of surface distortion minimization is used to determine the force sets required to bend in each of the 26 specified shapes and to give the residual distortion for each shape. The shapes are pseudo-bending modes for the mirror, based on solutions for an annular flat plate of similar dimensions. These shapes combine the convenience of being analytical functions, with reasonably low residual errors (e.g. much less than Zernikes). 117 of the 120 possible shapes obtained by applying unit forces at each of the axial supports are used to form the matrix of shapes, $[L]$, which is augmented by the addition of six rigid body shapes and power before performing the minimization. The minimization is performed 26 times with one of the shapes being used as U_g each time. The residual error in terms of RMS surface normal displacement and surface slope is shown in Figure 22.

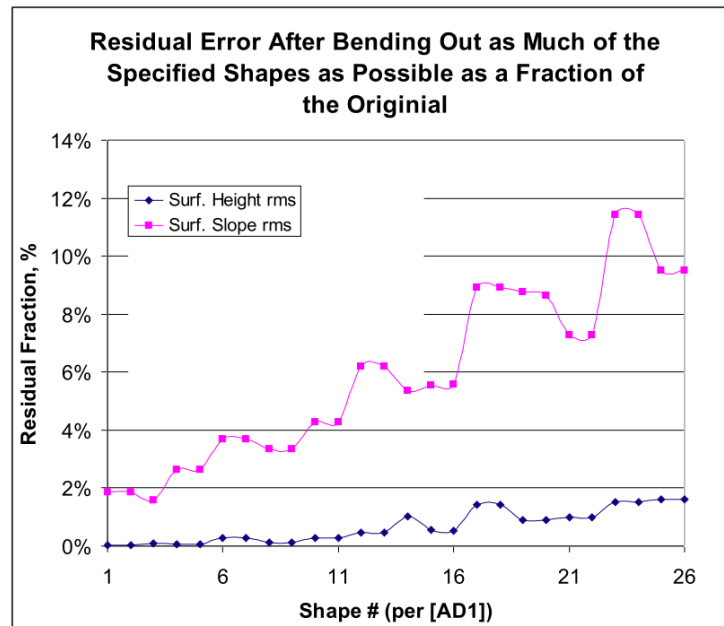


Figure 22. Surface normal and surface slope residual error after an optimal correction.

The surface distortion minimization method was also used to determine the coefficients of the 26 specified shapes that optimally correct mirror distortion under operational loads. In this case, [L] is formed from the 26 defined shapes plus the rigid body shapes and power and U_g is the raw displacement result to be corrected.

In practice it was found that certain combinations of bending modes were similar to focus and coma, confusing surface figure and collimation errors. For example, the two axisymmetric bending modes can fit focus with less than 10% residual. To the extent that small errors fit these residuals they would be amplified into large rigid body and complimentary bending demands. For both the focus and coma cases, the bending modes involved include a soft low order mode and a much stiffer higher order mode; to avoid the artificial creation of high bending force demands the higher order mode may be selectively dropped from the wavefront solution above a certain noise threshold.

The specified shapes cannot be bent in perfectly so the scaled residual for each shape is RSS'd with the calculated surface distortion obtained by subtracting the scaled shapes from the raw displacement to arrive at the net rms surface normal and slope error.

In some operating modes surface distortions may have changed since the surface was last measured. We estimate the amount of such surface changes by keeping track of the repeating and non-repeating support error force components. Distortions caused by unsteady wind loading are also uncorrectable. For these distortions only the rigid body shapes and power are subtracted. The surface distortion minimization operation is performed on each individual load case, approximately 150 load cases are considered consisting of gravity and actuator error force cases. Most cases are unit load cases and the optimization described above is applied with only rigid body shapes removed and a second time with rigid body and 25 of the 26 defined shapes removed (with residual errors added back in). The results of these operations, rms surface slope error for each load case, is combined with the estimated repeating and non-repeating error forces as described below.

8. CALCULATION OF NET MIRROR DISTORTION ATTRIBUTABLE TO THE SUPPORT SYSTEM

The performance analysis for the primary mirror support follows a similar process to that of the LSST mirror supports³. The analysis considers the effect of force and moment errors at every attachment point to the mirror, and the correctability of those errors, either by calibration in open-loop mode or by wavefront sensing based feedback in closed-loop mode.

8.1 Support force errors

Support force errors are the difference from the intended value of any of the six force components (F_x , F_y , F_z , M_x , M_y and M_z) possible at an actuator interface point on the mirror. Error forces result from misalignment and from frictional or elastic effects. Misalignment and elastic error forces will not change over time so the distortion they produce can be measured and corrected. This is less likely to be true of frictional error forces. We categorize error forces that do not change unpredictably between distortion measurement and corrections as repeating error forces. Those that might change between measurements are categorized as non-repeating error forces. The effects of repeating error forces can be partially corrected by the AOS system.

The repeating and non-repeating error forces for the primary axial and lateral support actuators have been estimated and prototypes have been tested to validate the actuator design. The lateral support actuators are not involved in the active correction of distortion, this task is left to the 120 axial support actuators. Forces in the lateral system are adjusted to keep loads on the three tangent rods below budgeted levels. In the Prime Focus Assembly (PFA) configuration the primary mirror is displaced in piston and tilt to maintain collimation. This displacement results in systematic, repeatable changes in the lateral actuator support forces, mainly due to changes in the alignment of the connecting rods relative to the mirror. The effects of mirror displacement are evaluated by including the lateral support actuator connecting links in the primary mirror finite element model, shown in Figure 23, and displacing the mirror relative to its supports with the large deflection analysis option in ANSYS turned on.

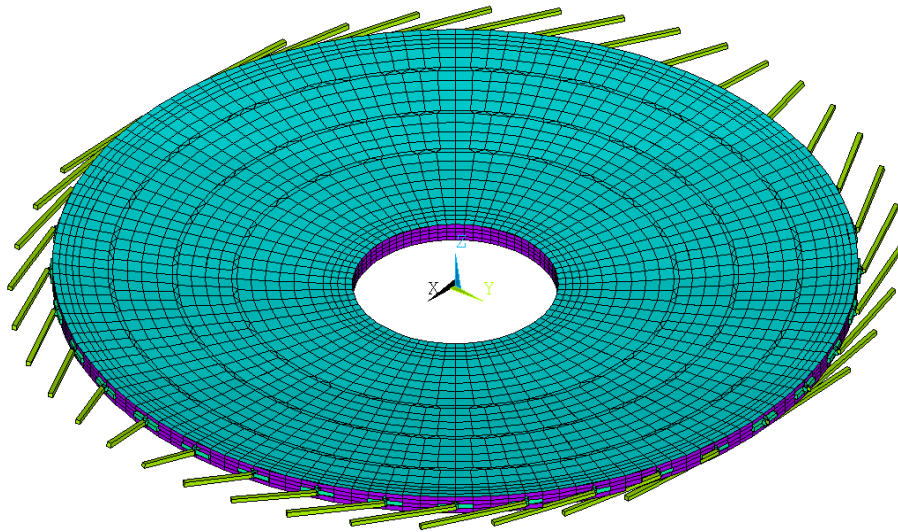


Figure 23. The DCT Primary Mirror finite element model with lateral support connecting links.

8.2 Randomly distributed support force errors

A random distribution of support force errors will generally be less damaging than a distribution that has a low order spatial distribution. We use the full actuator error force, repeating and non-repeating, in estimating the effect of randomly distributed force errors (we use a fraction of the error force in evaluating the effect of systematically distributed error forces with the fraction determined by a Monte Carlo Analysis).

Random support force errors are evaluated by sampling the effects at one location and using those results at all similar locations. The RMS slope error for the 36 axial actuators in the outer row caused by one of the error force components is simply $\sqrt{36}$ * the RMS slope error caused by the error force applied to one of these locations.

In most cases the applied error force is reacted by the kinematic constraints applied to the finite element model. Axial force errors are reacted by distributed axial forces at all actuators to mimic the response of the mirror support control system.

8.3 Systematically distributed support force errors

These are sets of forces acting on the mirror that are correlated in some way. Examples are forces that result from or are altered by differential thermal growth or a displacement of the mirror relative to the supports. These effects tend to produce force sets that have net radial, lateral or astigmatic components. Force sets that generate the low order flexural modes of the mirror can yield deflections that are much larger than would be predicted using the random support force analysis procedure above. Random chance can also result in error force distributions that result in low order distortions such as astigmatism. This effect is evaluated by performing a Monte Carlo analysis in which 100 sets of error forces are randomly assigned and each resulting force set is evaluated to determine how much of a low order distribution of force it contains.

Axial error forces make the largest contribution to distortion so attention will be confined to this component, including the axial error component from the lateral support actuators. It is assumed that the systematic distribution can be expressed as a linear combination of normalized force sets given by the bending mode polynomials evaluated at the actuator locations. These force sets are applied to the finite element model and RMS surface slopes are computed. The scaling factor to apply to each of these load cases has been calculated by generating 100 sets of randomly selected actuator forces and evaluating the coefficients for the Zernike components of each set. The standard deviation ($\hat{\sigma}$) of these coefficients gives the value that will not be exceeded 68% of the time, the average value is near zero as would be expected. In the case of the primary with 120 actuators, the standard deviation of the astigmatic force coefficient is 13% of the RMS value of the actuator force error. The standard deviations of the coefficients for other low order distributions are similar in magnitude. It is assumed that the $1/\hat{\sigma}$ force coefficient applies to each term simultaneously.

8.4 Repeating and non-repeating support force errors

As noted above, the finite element load cases were processed twice removing only rigid body shapes representing the effect of non-repeating error forces and removing also 25 defined shapes representing the effect of the repeating component of error force. We have also noted that we estimate the magnitudes of both the repeating and non-repeating error forces. We then compute the effect of repeating and non-repeating error forces and RSS the result together to obtain the net effect. Note that we could obtain the same result by applying the estimated error forces as the actual input to the finite element model. This would require separate load cases for the repeating and non-repeating error force magnitudes and a re-run whenever the force estimates were revised, a frequent occurrence since the support system design is refined in response to the analysis results.

8.5 Totaling the effects of all error sources

Gravity, random and non-random structure function errors are combined by RSS'ing all results of. Specifically:

Where: TM_{Total} is the net RMS slope error from the support system
 TM_g is the RMS slope error for gravity at a particular elevation angle.
 TM_{Random} is the net random error force slope error
 TM_A, TM_B, etc are the non-random cases

This equation applies equally to the RMS surface distortion.

8.6 Results

Predicted results in terms of primary surface slope error as a function of elevation angle when primary wavefront measurements are not available are shown in Figure 24. Although surface wavefront measurements are not available, the AOS can still make corrections for certain elevation angle dependent effects such as misalignment. Axial force adjustments may also be needed if the primary mirror position is changed to collimate the telescope. Figure 25 shows the improvement in figure when wavefront information is available. Note that much of the gravity error is quilting deformation that is polished out zenith pointing but re-appears when pointing off zenith. Figure 25 shows what the primary slope errors would be without the AOS. The benefit of the AOS system can be seen by comparing the primary slope errors in Figure 26 to those in Figures 24 and 25. Movement of the primary to re-collimate the telescope results in large surface slope errors unless axial support forces are adjusted. Even if the primary position relative to the cell is fixed, the surface slope error when Zenith pointing degrades from 0.03 arc-sec-RMS to 0.08 arc-sec-RMS without the axial force adjustments provided by the AOS system.

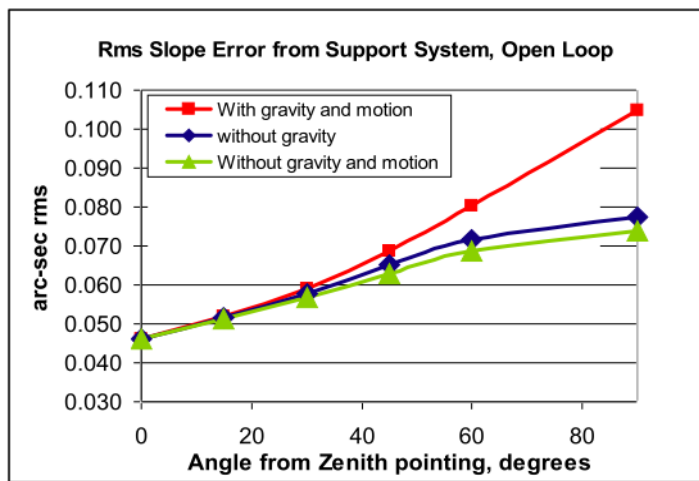


Figure 24. Primary surface rms slope error as a function of elevation angle when surface wavefront information is not available.

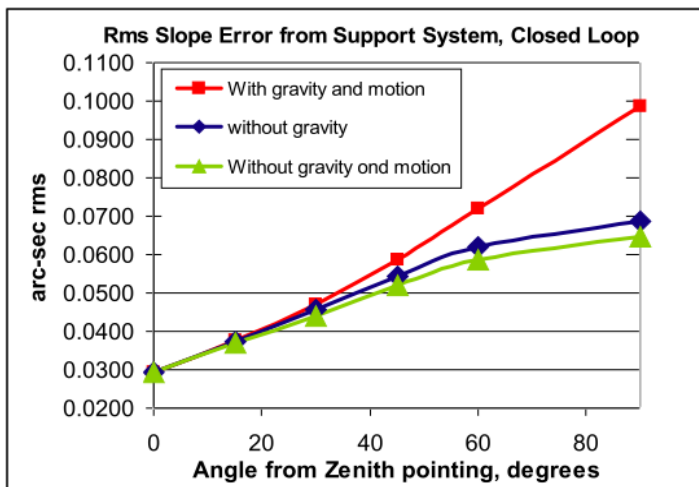


Figure 25. Primary surface rms slope error as a function of elevation angle when surface wavefront information is available.

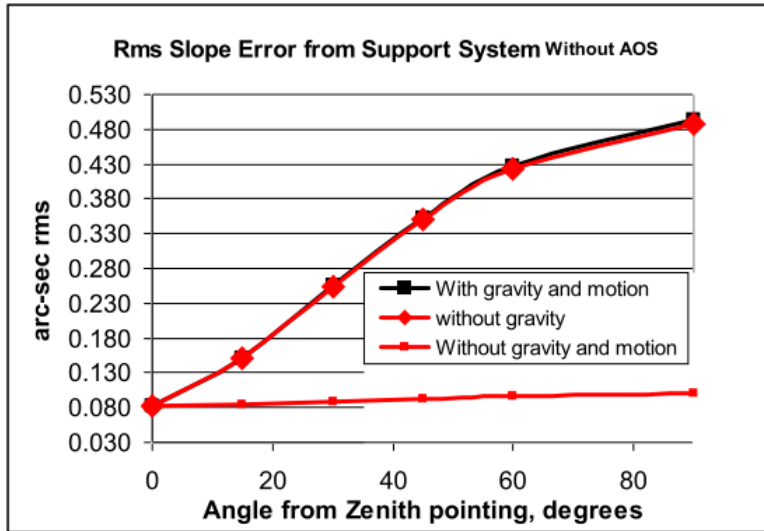


Figure 26. Primary surface rms slope error as a function of elevation angle without an AOS. movement of the primary relative to the cell results in a large increase in slope error but even if the mirror is fixed in position, slope error increases from 0.03 to 0.07 arc-sec-rms to 0.08 to 0.1 arc-sec-rms not including gravity effects.

REFERENCES

- [1] Schwesinger, G., "Lateral support of very large telescope mirrors by edge forces only," *Journal of Modern Optics*, 38(8), 1507-1516 (1991).
- [2] Lotz, P., "Discovery Channel Telescope software key technologies," *Proc. SPIE 7740* (2010).
- [3] Cuerden, B., Sebag, J., Mathews, S., Cho, M., Lee, J. and West, S., "LSST primary, secondary and tertiary mirror support systems," *Proc. SPIE 5495*, 474 (2004).